Global structure of ground-state phase diagrams in the one-dimensional anisotropic extended Hubbard model

Hiromi Otsuka*
Department of Physics, Tokyo Metropolitan University, Tokyo 192-0397, Japan
(Received 24 March 2000; revised manuscript received 14 August 2000; published 12 March 2001)

We discuss global structures of ground-state phase diagrams in a one-dimensional half-filled electron system with on-site and spin-dependent nearest-neighbor-site Coulomb interactions. We compare our numerical calculation data for phase boundary lines with their analytical expressions in three limiting regions of interaction parameters and find good agreement between them. In the intermediate-coupling region, however, we observe nontrivial structures of phase diagrams: For systems with weak easy-plain anisotropy, both the bond-located spin- and charge-density-wave phases are realized. The latter contacts with the ferromagnetic phase stabilized in the strong-coupling region. On the other hand, when anisotropy becomes large, the intermediate phase disappears and consequently a direct transition between the former and ferromagnetic phase is observed.

DOI: 10.1103/PhysRevB.63.125111 PACS number(s): 71.10.Hf, 71.30.+h, 74.20.Mn

I. INTRODUCTION

So far, interacting electron systems have attracted great interest in the research of electric and magnetic properties of materials.[1] Especially, since the discovery of the high-T_c superconductor, two-dimensional (2D) electron systems have been intensively studied and a large number of investigations have been devoted to the understanding of many-body effects caused by electron correlations. But in general, since precise descriptions on the low-energy and long-distance behaviors of systems should be required as a first step, it is quite difficult to understand them. In investigating one-dimensional (1D) quantum systems, however, the Tomonaga-Luttinger liquid (TLL) picture was established on the basis of conformal field theory (CFT), which now permits us to describe low-energy physics more accurately than before.[2–4] In this situation, it is naturally expected that precise understandings on 1D interacting electron systems should throw some light upon problematic researches of 2D systems.[5]

The 1D extended Hubbard model (EHM) including the nearest-neighbor Coulomb interaction has been recognized as the simplest but relevant model to 1D materials; its Hamiltonian is $H_{\mathrm{EHM}}=H_{\mathrm{HM}}+H_{\mathrm{E}}$ with

$$H_{\mathrm{HM}}=\sum_{j,s=\pm}-t(c^{\dagger}_{j,s}c_{j+1,s}+\mathrm{H.c.})+\frac{U}{2}n_{j,+}n_{j,-}, \quad (1)$$

$$H_{\mathrm{E}}=\sum_{j}Vn_jn_{j+1}, \quad (2)$$

where $c_{j,s}$ annihilates an electron with spin s on jth site and $n_{j,s}\equiv c^{\dagger}_{j,s}c_{j,s}$ (H_{HM} is the Hubbard Hamiltonian). Using $\mathbf{c}^{\dagger}_j\equiv(c^{\dagger}_{j,+},c^{\dagger}_{j,-})$, a charge on jth site is $n_j\equiv\mathbf{c}^{\dagger}_j\cdot\mathbf{c}_j$. For example, the half-filled EHM was recently used to describe low-energy features of Sr_2CuO_3 observed in the electron energy-loss spectroscopy (EELS) measurement; the model parameters were determined as $t=0.55$ eV, $U=4.2$ eV, and $V=1.3$ eV.[6]

On the other side, investigations on ground-state properties have been intensively performed: At half filling, Fourcade and Spronken[7] found a continuous transition between the spin-density-wave (SDW) and charge-density-wave (CDW) states near the $2V=U>0$ line by use of real-space renormalization-group (RG) and exact diagonalization methods. While continuum field theory[8] (perturbative approaches[9]) predicts SDW-CDW transition to take place on $2V=U$ line in the weak-coupling (strong-coupling) limit, Hirsch,[10] employing a quantum Monte Carlo simulation method, clarified that it occurs at a certain value $2V^*$ larger than U, which is in accord with the above-mentioned calculation results, and further he found a crossover from a continuous to first-order transition at a point $2V\simeq U\simeq 3$ (with taking t as energy unit). Following these, many numerical investigations[11–14] as well as analytical ones[15,16] have been performed to obtain quantitatively reliable phase diagrams, but mainly due to limitations in usable approaches, precise understanding on this model was not obtained.

Quite recently, Nakamura[17,18] investigated half-filled EHM by employing the so-called ''level-spectroscopy'' method[19] and predicted a remarkable phase diagram, where an existence of the intermediate ''bond-located'' CDW phase (to be defined below) is exhibited in the weak- and intermediate-coupling regions. Further it was conjectured that the above-mentioned crossover is realized on a confluent point of continuous transition lines in charge and spin parts. This novel method which was initiated by Jullien and Haldane[20] and extensively developed by Nomura and Okamoto[21] is based upon CFT, RG, and symmetry properties of excitations observed in TLL. And it is being recognized as powerful in investigations of 1D electron systems[17,18,22,23] as well as quantum spin chains.[24–26]

Following these developments, the present author has recently investigated many-body effects of spin-dependent non-point-like Coulomb interactions through the 1D half-filled ''anisotropic'' extended Hubbard model (AEHM) defined by the Hamiltonian: $H_{\mathrm{AEHM}}=H_{\mathrm{HM}}+H_{\mathrm{AE}}$ with

$$H_{\mathrm{AE}}=\sum_{j,s=\pm}(V_1n_{j,s}n_{j+1,s}+V_2n_{j,s}n_{j+1,-s}) \quad (3)$$

 ©2001 The American Physical Society

in the repulsive case (U, $V_{1,2}>0$).[27] There we parametrized spin-dependent Coulomb interactions as $V_{1,2}=V(1\mp\delta)$ (the upper sign refers to the former in such expressions). Then $H_{\rm AEHM}$ expresses EHM with a U(1)-symmetric exchange coupling $-4\delta V S_j^z S_{j+1}^z$, so the system acquires easy-plain or easy-axis anisotropy depending on the sign of δ. Here $S_j^\mu \equiv \frac{1}{2}\mathbf{c}_j^\dagger \cdot \sigma^\mu \cdot \mathbf{c}_j$ is the spin operator on jth site (σ^μ is the μth Pauli matrix). This model was originally introduced as the simplest one for excitonic insulators[28] characterized by the existence of nonzero local charge or spin currents and the g-ology arguments on this model were performed.[29] In the previous paper, we numerically determined transition points and constructed ground-state phase diagrams of AEHM with weak anisotropy ($-0.1\leqslant\delta\leqslant 0.2$) in the weak- and intermediate-coupling regions ($0\leqslant U\leqslant 5$).[27] We then observed that while the bosonization prediction accurately reproduces our data in the weak-coupling limit, calculated boundaries considerably deviate from it with the increase of interactions. Especially, in the easy-plain anisotropy region, we found a crossing of boundary lines which provides a multicritical point of four phases. In the easy-axis anisotropy region, the intermediate bond-located CDW phase is observed which is the same as the abovementioned EHM case.[17,18]

While our previous research was restricted to the weak anisotropy systems in the weak- and intermediated-coupling regions, quantitatively reliable phase diagrams in entire region of interaction parameters are desired. Therefore, in this paper, we present global structures of the ground-state phase diagrams of AEHM and clarify the spin-dependent non-point-like Coulomb interaction effects on 1D electron systems. The organization of this paper is as follows. In Sec. II, using effective Hamiltonians in three limiting regions, i.e., the weak-coupling (U, $V<1$), spin-limit ($U\gg 1$, $V<1$), and strong-coupling (U, $V\gg 1$) regions, we analytically describe some possible scenarios of phase transitions. In Sec. III, we explain numerical calculation methods by which transition lines predicted in Sec. II are accurately determined. In Sec. IV, we show phase boundaries obtained by numerical calculations, which will be closely compared to those given in Sec. II. To serve a reliability of our calculations, we also perform a consistency check among different types of excitations. Section V is devoted to discussions and summary of the present investigation; a characterization of phases will be performed by using order parameters corresponding to electron excitations.

II. THREE LIMITING REGIONS

A. Weak-coupling region (U, $V<1$)

First we summarize scenarios of phase transitions in the weak-coupling region. In studying 1D electron systems, the following bosonization identity[30] is quite useful: $c_{j,s} \to \Sigma_{r=\pm} e^{rik_{\rm F}x}\psi_{r,s}(x)$ with

$$\psi_{r,s}(x)=\frac{1}{\sqrt{2\pi\alpha}}e^{i[r(\phi_\rho+s\phi_\sigma)-(\theta_\rho+s\theta_\sigma)]/\sqrt{2}}. \tag{4}$$

Here the Fermi wave number $k_{\rm F}\equiv\pi n/2$ taking the lattice constant $a=1$, an electron density $n\equiv N/L$ and L (N) is the number of sites (electrons). The index $r=+$ ($-$) denotes the right-going (left-going) branch of the linearized cosine-band and α is a short distance cutoff. The bosonic operator θ_ν ($\nu=\rho$ or σ) is the dual field of ϕ_ν and satisfies the commutation relation $[\phi_\nu(x),\partial_y\theta_{\nu'}(y)]=i\pi\delta(x-y)\delta_{\nu,\nu'}$. According to the bosonization procedure,[8,31] the phase Hamiltonian of AEHM is extracted; at half filling $n=1$, it consists of the following three parts: $\mathcal{H}=\mathcal{H}_\rho+\mathcal{H}_\sigma+\mathcal{H}_{\rm e}$,

$$\mathcal{H}_\nu=\frac{v_\nu}{2\pi}\int dx\left[K_\nu(\partial_x\theta_\nu)^2+\frac{1}{K_\nu}(\partial_x\phi_\nu)^2\right] + \frac{2g_\nu}{(2\pi\alpha)^2}\int dx\cos\sqrt{8}\phi_\nu, \tag{5}$$

$$\mathcal{H}_{\rm e}=\frac{2g_{3\parallel}}{(2\pi\alpha)^2}\int dx\cos\sqrt{8}\phi_\rho\cos\sqrt{8}\phi_\sigma. \tag{6}$$

Here K_ν and v_ν are the Gaussian coupling and the velocity of elementary excitations. Three parameters g_ρ, g_σ, and $g_{3\parallel}$ stand for the Umklapp scattering, the backward scattering, and a spin-charge coupling, respectively; they may take systems out of the TLL universality class. According to the RG argument,[15] the energy scale of $\mathcal{H}_{\rm e}$ is larger than those of the others; we thus suppose that $\mathcal{H}_{\rm e}$ is irrelevant at least in the weak-coupling region so that spin-charge separation occurs. Consequently, each degree of freedom is described by the quantum sine-Gordon model (QSGM) Hamiltonian $\mathcal{H}_\nu$.

The RG equations for $\mathcal{H}_\nu$ are derived by changing the short distance cutoff constant as $\alpha\to\alpha e^{dl}$; then the Berezinskii-Kosterlitz-Thouless (BKT) type equations are obtained within the one-loop calculation:[32]

$$\frac{dy_{\nu,0}(l)}{dl}=-y_{\nu,1}^2(l),\quad \frac{dy_{\nu,1}(l)}{dl}=-y_{\nu,0}(l)y_{\nu,1}(l), \tag{7}$$

where $y_{\nu,0}=2(K_\nu-1)$ and $y_{\nu,1}=g_\nu/\pi v_\nu$. Figure 1 gives the schematic RG-flow diagram. Since the bosonization procedure leads the following relations between these parameters and those in the original Hamiltonian $H_{\rm AEHM}$, i.e., $2\pi v_{\rm F}(K_{\rho,\sigma}-1)\simeq\mp(U\pm 4V_1+2V_2)$ and $g_{\rho,\sigma}\simeq(U-2V_2)$ (notice that to get the latter relation, the origin of ϕ_ρ was appropriately shifted), we can get types and approximate points of phase transitions as follows. Let us see the system with increasing V, but keeping δ and U fixed (i.e., along the arrows in Fig. 1). In the easy-axis anisotropic case $\delta<0$, one finds that both charge and spin parts are massive except for a point $y_{\nu,1}=0$ ($y_{\nu,0}<0$), i.e.,

$$2V_{\rm G}^*\simeq\frac{U}{1+\delta}, \tag{8}$$

where the Gaussian-type second-order transition occurs. In the easy-plain anisotropic case $\delta>0$, the critical point Eq. (8) and the type of the transition do not change in the charge part, but the spin part is expected to realize the hidden-SU(2) BKT transition on the line $y_{\sigma,0}=-y_{\sigma,1}>0$, thus

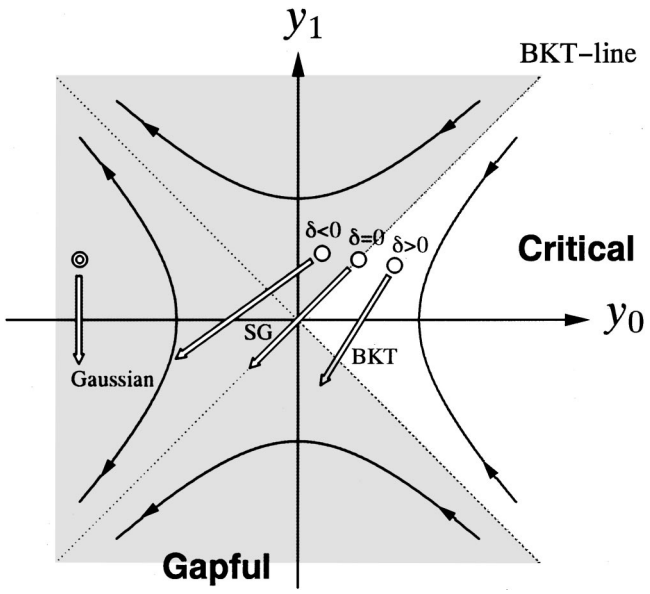

FIG. 1. Schematic representation of RG-flow diagram of QSGM (we dropped the index ν). Right three arrows show trajectories of bare couplings in the spin part (with the increase of V but δ and U fixed). Double circle with an arrow corresponds to the charge part.

$$2V^*_{\mathrm{BKT}} \simeq \frac{U}{1-\delta}, \tag{9}$$

which follows the stable Gaussian fixed point Eq. (8).

B. Spin-limit region ($U \gg 1$, $V<1$)

Next, we consider the region $U \gg 1$ and $V<1$ where charge fluctuations are almost suppressed. An effective model in this limit is the $S=\frac{1}{2}$ XXZ chain defined by the Hamiltonian

$$\mathcal{H}_{XXZ} = J\sum_j \left(S^x_j S^x_{j+1} + S^y_j S^y_{j+1} + \Delta S^z_j S^z_{j+1}\right), \tag{10}$$

where $J \simeq 4/U$ and $\Delta \simeq 1-\delta VU$. Now since the exact solution for this effective Hamiltonian is given by the Bethe-ansatz method,[33] we can draw phase boundaries of AEHM in this limit. For $-1<\Delta \leqslant 1$ the ground state of $\mathcal{H}_{XXZ}$ is in the spin-liquid phase where the Gaussian coupling K_σ is given as[34,35]

$$K_\sigma = \frac{2}{1+(2/\pi)\sin^{-1}\Delta}. \tag{11}$$

After the BKT transition at $\Delta=1$, the Néel phase is realized in $1<\Delta$. This inequality is always satisfied (unsatisfied) in the easy-axis (easy-plain) anisotropic case. On the other hand, the condition $\Delta=-1$ where K_σ diverges to $+\infty$ is known to define the first-order phase transition point between the liquid and ferromagnetic phases, so it provides a phase boundary for AEHM

$$V^*_{\text{F-SDW}} \simeq \frac{2}{\delta U}, \tag{12}$$

which separates the ferromagnetic phase from a SDW-type one in the easy-plain anisotropic case.

In addition to the phase transition lines, a condition $\Delta=0$ [i.e., the $S=\frac{1}{2}$ XY chain ($K_\sigma=2$)] expresses a point on the stable Gaussian fixed line in this region; for AEHM this is rewritten as

$$V_{XY} \simeq \frac{1}{\delta U}. \tag{13}$$

We expect that this line behaves as Eq. (8) in the weak-coupling region. In Sec. IV C we shall perform a consistency check of numerical calculation data on this line.

C. Strong-coupling region ($U, V \gg 1$)

Last we consider the strong-coupling region where the kinetic energy of electrons is negligible compared to the Coulomb potential energy, so the effective Hamiltonian is given by

$$\mathcal{H}_{\mathrm{cl.}} = \sum_j \left(Un_{j,+}n_{j,-} + Vn_jn_{j+1} - 4\delta VS^z_jS^z_{j+1}\right). \tag{14}$$

This model is diagonal in the configuration space of electrons. For $\delta=0$ two types of ground states are realized, i.e., the twofold degenerate CDW state (energy $E_{\mathrm{CDW}}=\frac{1}{2}LU$) and a 2^L-fold degenerate spin-state with all sites singly occupied ($E_{\mathrm{spin}}=LV$). These two types of states are separated by the first-order transition line $2V=U$. When δ takes a nonzero positive (negative) value, the ferromagnetic (Néel) state fully gains the energy through the U(1)-symmetric exchange coupling as E_{F} ($E_{\text{Néel}}$)$=LV(1-|\delta|)$, and thus the degeneracy of spin-state is lifted, although E_{CDW} is unchanged. Consequently we can estimate a phase boundary between the ferromagnetic (Néel) and CDW states as

$$2V^*_{\text{F-CDW,N-CDW}} \simeq \frac{U}{1\mp\delta} \tag{15}$$

up to leading order in U and V (although more accurate estimations are possible using perturbation calculations, we employ this expression in the following sections). In the easy-plain anisotropic case, the ferromagnetic phase boundary given by Eq. (15) is expected to behave as Eq. (12) in that limit. This can be directly confirmed through a comparison between numerical calculation data and limiting behaviors; we shall check this in Sec. IV B.

III. NUMERICAL CALCULATION METHODS

A. Continuous phase transitions

We have seen qualitative descriptions on phase transitions in AEHM, but for the aim of quantitative discussions on global structures of phase diagrams, numerical calculations are unavoidable. We employed the level-spectroscopy method to treat continuous phase transitions, i.e., Gaussian and hidden-SU(2) BKT ones. Therefore, in this subsection, we briefly summarize some relevant points of this method to

our calculations. A criterion to determine ferromagnetic transition points will be discussed in the next subsection.

Let us start with considering the following operators:

$$\mathcal{O}_{\nu,1} \equiv \sqrt{2}\cos\sqrt{2}\phi_\nu, \tag{16}$$

$$\mathcal{O}_{\nu,2} \equiv \sqrt{2}\sin\sqrt{2}\phi_\nu, \tag{17}$$

$$\mathcal{O}_{\nu,3} \equiv \exp(+i\sqrt{2}\theta_\nu), \tag{18}$$

where $\mathcal{O}_{\nu,1}$ and $\mathcal{O}_{\nu,2}$ denote ν-channel current excitations while $\mathcal{O}_{\nu,3}$ expresses those accompanied by the change of the total amount of ν. Here CFT says that in finite-size systems the excitation energy corresponding to these operators are expressed by their scaling dimensions $x_{\nu,i}$ as

$$\Delta E_{\nu,i} \simeq \frac{2\pi v_\nu}{L} x_{\nu,i} \tag{19}$$

($i=1$, 2, and 3), and further their behaviors are predicted on the basis of the operator product expansion technique.[36,37] In order to determine hidden-SU(2) BKT transition points, we should treat a finite-size system whose spin part is located near the line $y_{\sigma,0}=-y_{\sigma,1}\geqslant 0$. The renormalized scaling dimensions are then given as

$$x_{\sigma,1} \simeq \frac{1}{2} - \frac{1}{4} y_{\sigma,0}(l)(1+2t), \tag{20}$$

$$x_{\sigma,2} \simeq \frac{1}{2} + \frac{1}{4} y_{\sigma,0}(l)(3+2t), \tag{21}$$

$$x_{\sigma,3} \simeq \frac{1}{2} - \frac{1}{4} y_{\sigma,0}(l), \tag{22}$$

where a small parameter $t \equiv |y_{\sigma,1}|/y_{\sigma,0} - 1$.[19,21,38] Therefore the level crossing of $\Delta E_{\sigma,1}$ and $\Delta E_{\sigma,3}$ excitations may serve a good estimator for this transition. On the other hand, for a system near the Gaussian fixed line (i.e., for a small $|y_{\nu,1}|$ value),

$$x_{\nu,1} \simeq \frac{1}{2} + \frac{1}{4} y_{\nu,0}(l) + \frac{1}{2} y_{\nu,1}(l), \tag{23}$$

$$x_{\nu,2} \simeq \frac{1}{2} + \frac{1}{4} y_{\nu,0}(l) - \frac{1}{2} y_{\nu,1}(l), \tag{24}$$

$$x_{\nu,3} \simeq \frac{1}{2} - \frac{1}{4} y_{\nu,0}(l). \tag{25}$$

We can thus obtain points on the Gaussian fixed lines from the level crossing of $\Delta E_{\nu,1}$ and $\Delta E_{\nu,2}$ excitations.

To proceed, we should connect the above discussion to numerically accessible quantities; this was accomplished by Nakamura *et al.*[17,18,22] There, discrete symmetries of a lattice Hamiltonian, (e.g., translation, space inversion and spin reverse) are utilized to characterize a state generated by an operation of $\mathcal{O}_{\nu,i}$ on the ground state. Classification of operators with respect to the symmetries was then performed, and the result was summarized in Table I of Ref. 17. Therefore, by employing it, we can directly extract elementary-excitation levels $\Delta E_{\nu,i}$ through exact diagonalization calculations of AEHM under a properly taken boundary condition.

B. First-order phase transition to complete ferromagnetic state

We in this subsection explain the numerical method to determine the first-order transition line to the complete ferromagnetic phase which is expected to occur in easy-plain anisotropic systems. As we have seen in Sec. II B, this transition is characterized by the divergence of the Gaussian coupling $K_\sigma \to \infty$ in the spin-limit. Actually for the phase-separation transition observed in the 1D *t-J* model which is a well-known example as the same kind of transition ($K_\rho \to \infty$ in that case), Ogata *et al.* evaluated the boundary line via the divergent behavior of the charge compressibility in exact diagonalization calculation data.[39] This approach is valid for the SDW-ferromagnetic phase transition, but for the CDW-ferromagnetic phase transition in the strong-coupling region, since K_σ cannot be defined, we should employ some other criterion.[40]

Recently, Hirata and Nomura[41] studied the $S=\frac{1}{2}$ frustrated *XXZ* chain in the ground state, where transitions from the dimer and *XY* phases to the ferromagnet were successfully treated, and further, same approach was applied to determine the first-order transition lines observed in an extended Hubbard model[18,42] with site-off-diagonal interactions.[43] Their way of determining the boundary is quite simple; namely, the condition that the ground-state energy in the subspace of the z component of total spin $S^z_{\mathrm{T}}=0$ $[E_0(S^z_{\mathrm{T}}=0)]$ equals the fully magnetized state energy[44] provides a good estimation on the ferromagnetic phase transition point. In our AEHM case, since the complete ferromagnetic state is an eigenstate and its energy was given as E_{F} in Sec. II C, this condition is expressed as

$$\delta E_{\mathrm{F}} \equiv E_0(S^z_{\mathrm{T}}=0) - E_{\mathrm{F}} = 0. \tag{26}$$

In the following numerical calculations, we shall employ this criterion and determine the ferromagnetic phase boundary, which is closely compared to analytical expressions in limiting regions.

IV. RESULTS

A. Level structures

In this research we treat up to 16 sites systems, where the Lanczos algorithm was used to obtain eigenvalues of the Hamiltonian in each specified subspace. Then by extrapolating crossing points to the thermodynamic limit by use of the least square fitting procedure, various phase boundaries are evaluated. So we first demonstrate the Coulomb interaction parameter dependence of level structures.

In Figs. 2 and 3, we exhibit relevant excitation spectra. As expected, for systems whose charge part is near the unstable Gaussian fixed line, $\Delta E_{\rho,1}$ and $\Delta E_{\rho,2}$ possess a crossing point (Fig. 2), which is close to V^*_{G} (vertical dotted lines) in the weak coupling, but, with the increase of U, the difference

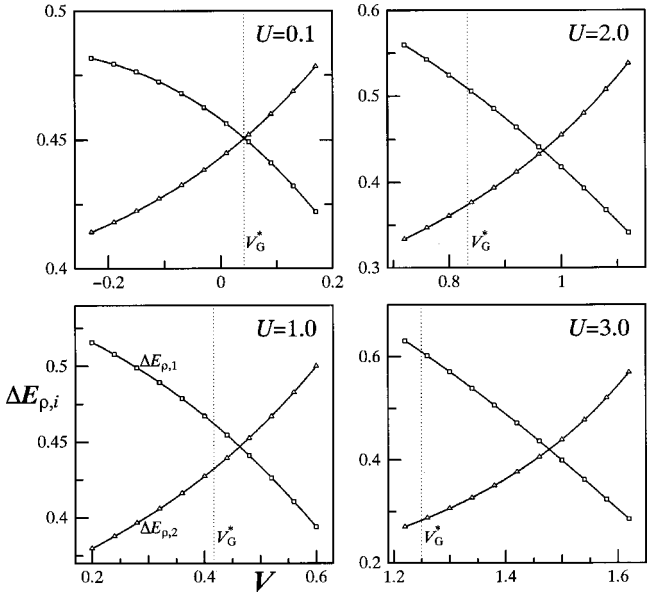

FIG. 2. V dependence of excitation levels $\Delta E_{\rho,1}$ (squares) and $\Delta E_{\rho,2}$ (triangles) observed in the systems whose charge part is near the unstable Gaussian fixed line ($L=14$ and $\delta=0.2$). Vertical dotted lines denote values of V_{G}^{*}.

becomes prominent. Figure 3 plots $\Delta E_{\sigma,i}$ near the stable Gaussian and hidden-SU(2) BKT transition lines. As clearly exhibited, with the increase of V, $\Delta E_{\sigma,1}$ and $\Delta E_{\sigma,2}$ first provide a crossing point indicating the stable Gaussian fixed line. There $\Delta E_{\sigma,3}$ is smaller than the others. After that, the level crossing between $\Delta E_{\sigma,1}$ and $\Delta E_{\sigma,3}$ occurs and gives an approximate estimation on the BKT transition point. As a result, what we have observed in these figures is in accord

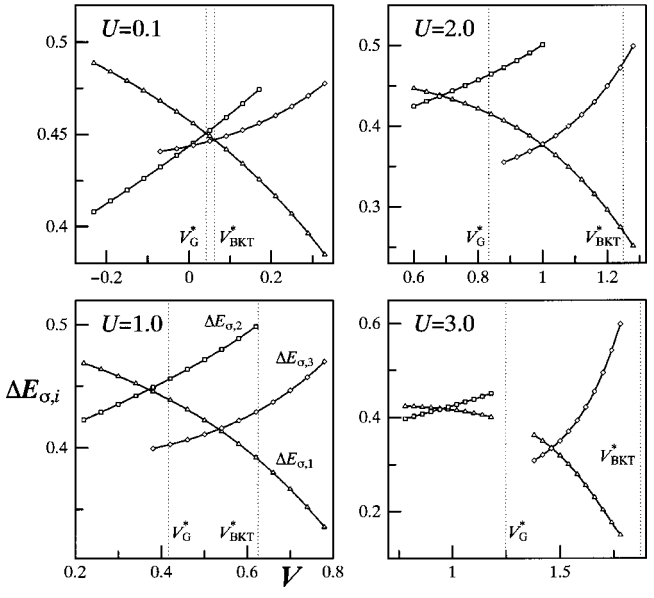

FIG. 3. V dependence of excitation levels $\Delta E_{\sigma,1}$ (triangles), $\Delta E_{\sigma,2}$ (squares), and $\Delta E_{\sigma,3}$ (diamonds) observed in the systems whose spin part is near the stable Gaussian and hidden-SU(2) BKT lines ($L=14$ and $\delta=0.2$). Vertical dotted lines denote values of V_{G}^{*} and V_{BKT}^{*}.

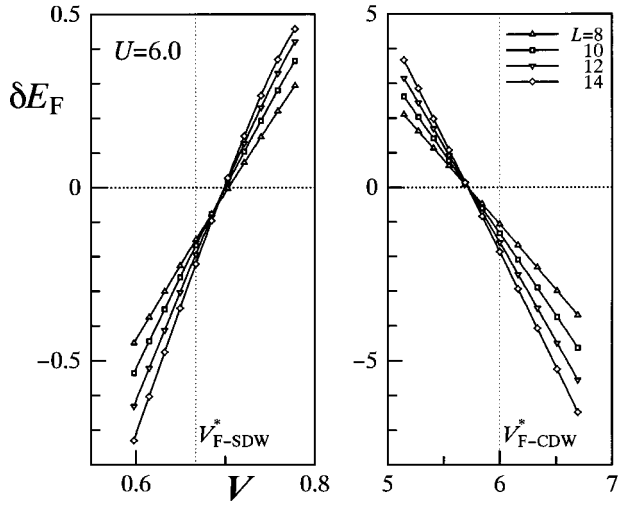

FIG. 4. V dependence of the energy difference δE_{F} ($\delta=0.5$ and $U=6$). The correspondence between marks and system sizes is given in the figure. Vertical dotted lines show $V_{\text{F-SDW}}^{*}$ and $V_{\text{F-CDW}}^{*}$.

with the scenario in Sec. II A and expressions on the renormalized scaling dimensions Eqs. (20)–(25). In Fig. 4, we plot δE_{F} the energy difference between the ground state and the complete ferromagnet in the spin-limit and strong-coupling regions ($\delta=0.5$, $U=6$, and up to $L=14$). From this figure, roughly speaking, the system with $U=6$ and within $0.7\lesssim V\lesssim 5.7$ is in the ferromagnetic state at this anisotropy parameter value.

Next we shall exhibit extrapolations of crossing points $V^{*}(L)$ to the thermodynamic limit. Figures 5 and 6 show cases of the Gaussian and hidden-SU(2) BKT transitions in charge and spin parts, respectively. While an important finite-size correction may stem from irrelevant fields with the

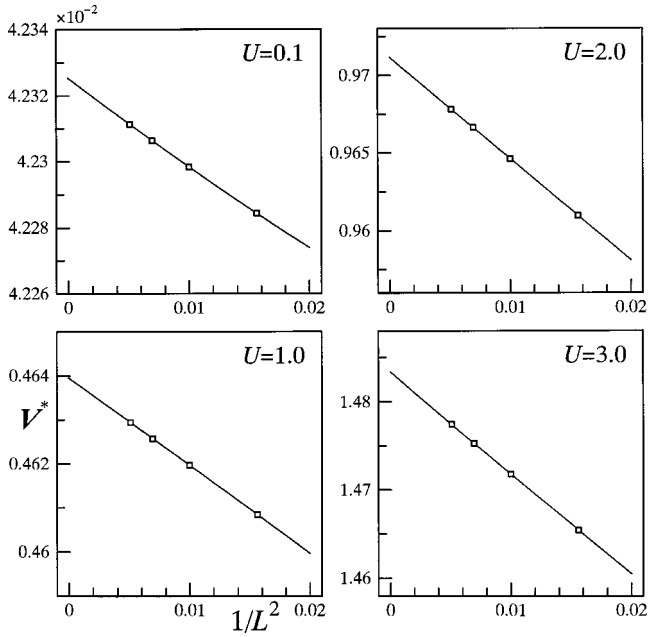

FIG. 5. System-size dependences of crossing points V^{*} evaluating the Gaussian transition points in the charge part ($\delta=0.2$). Curves show fitting lines.

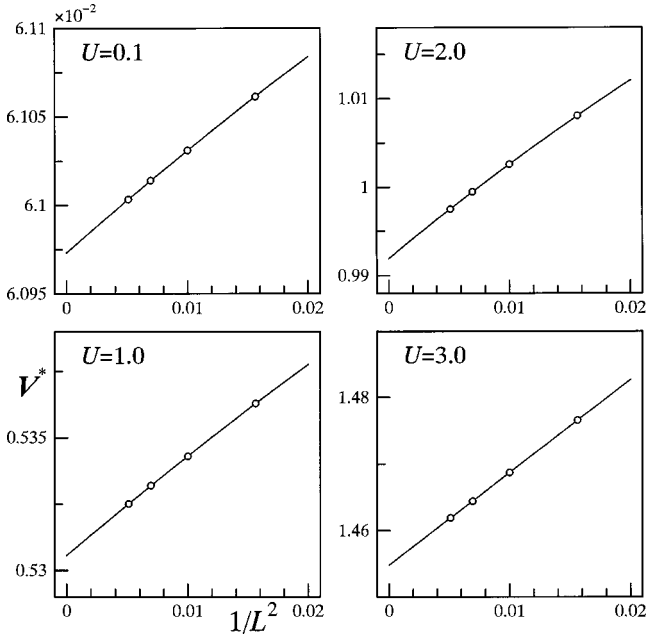

FIG. 6. System-size dependences of crossing points V^* evaluating the hidden-SU(2) BKT transition points in the spin part ($\delta=0.2$). Curves show fitting lines.

scaling dimension $x=4$,[21,36] and in fact, a linearity of the size dependence is visible in these figures, there must be some other complicated corrections, [e.g., $\ln(\ln L)$, $(\ln L)^2$, etc.]. In this research, we assume a form $V^*(\infty)+aL^{-2}+bL^{-4}$ for extrapolations; this may be evaluated through comparisons with analytical results in limiting regions. In the case of ferromagnetic transitions, a size dependence is almost absent except for the intermediate-coupling region where, as we shall see in the following, influences from other phases exist. Therefore we shall perform the numerical diagonalization calculations also for the 16-site system in this area.

B. Phase boundary lines

In Fig. 7, we show global structures of ground-state phase diagrams of AEHM with the anisotropy parameter values $\delta=0.2$ and 0.5. The triangles, squares, and circles with broken lines indicate the positions of the first-order transition to the ferromagnet, the Gaussian transition in the charge part and the hidden-SU(2) BKT transition in the spin part, respectively. Adding these, we also show the stable Gaussian fixed lines in the spin part by circles with dotted line. Magnifications of phase diagrams around the $2V=U$ line are also given in Fig. 8.

In the previous research, we calculated phase boundaries in weak- and intermediate-coupling regions and found that our data agree well with Eqs. (8) and (9).[27] Now from this figure we find that, independently to the values of δ, numerical calculation data excellently agree with the analytical expressions Eqs. (12), (13), and (15) also in the other two limiting regions. Consequently these observations may show the validity of our numerical approach given in Sec. III as well as discussions using effective Hamiltonians in Sec. II. On the other hand, for the strongly anisotropic case, $\delta=0.5$, we newly find that the crossing point of Gaussian and hidden-SU(2) BKT transition lines which is observed in weak easy-plain anisotropic cases disappears. This means that the ferromagnetic region contacts with a phase different from that in the $\delta=0.1$ and 0.2 cases around $2V=U$ line (see Fig. 8); we shall discuss this point in Sec. V.

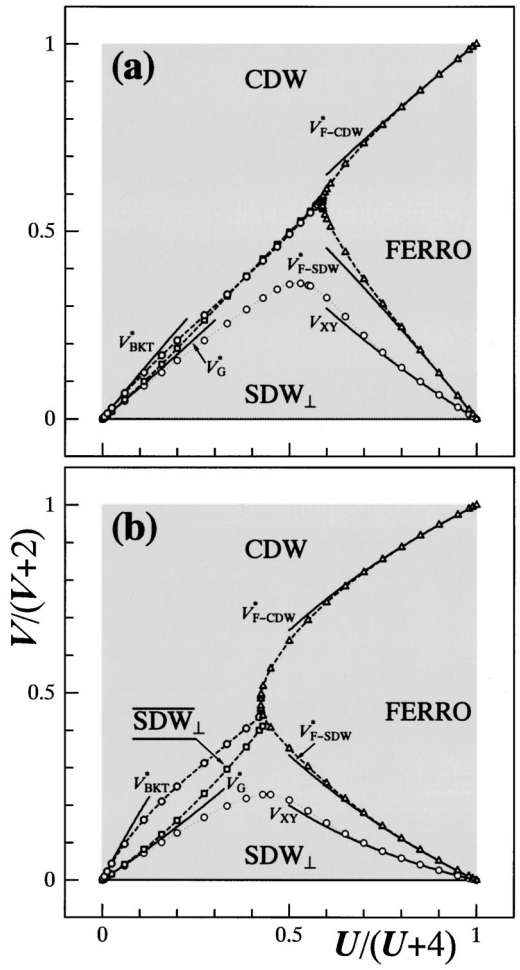

FIG. 7. Ground-state phase diagrams of the 1D AEHM at half filling: The easy-plain anisotropic cases (a) $\delta=0.2$ and (b) $\delta=0.5$. Solid curves denote analytically evaluated phase boundaries in Sec. II (we also draw V_{XY}). Triangles, squares, and circles with broken lines show the numerical results for the first-order transition to the ferromagnet, the Gaussian transition in the charge part, and the hidden-SU(2) BKT transition in the spin part, respectively. Stable Gaussian fixed line in the spin part is also exhibited by circles with dotted line.

Next we exhibit the data in the easy-axis anisotropic case ($\delta=-0.1$), where the Gaussian transition is expected in both charge and spin parts. Figure 9 plots phase boundaries, where squares and circles represent the data for the charge and spin parts, respectively. We find that $V^*_{\text{N-CDW}}$ also shows an excellent agreement with the data in the strong-coupling limit as well as V^*_{G} presenting good estimation on the boundary lines in the weak-coupling limit.[27] As we can see, with U taking a nonzero value, the phase boundary splits into two Gaussian-type transition lines. Then these lines appear to be

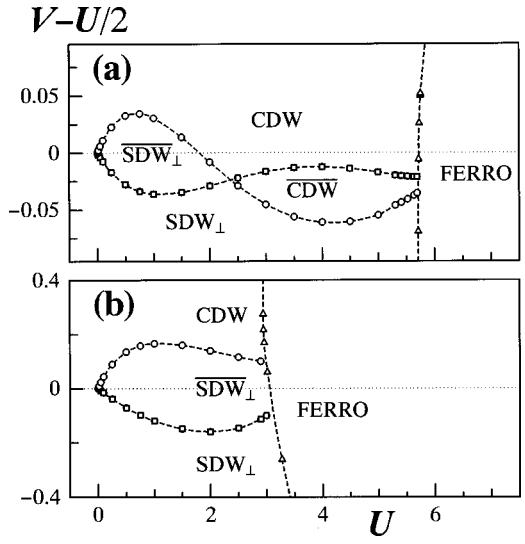

FIG. 8. Magnifications of ground-state phase diagrams close to the $2V=U$ line: Easy-plain anisotropic cases (a) $\delta=0.2$ and (b) $\delta=0.5$.

confluent to a single line around $U\simeq 10$. This behavior is qualitatively same as the EHM case[17,18]; an implication of this confluence is referred to in Sec. V.

C. Consistency checks

In this subsection we present consistency-check results among various types of excitations indexed by the symmetries of states. This procedure is, as we see below, based upon the finite-size corrections in the TLL universality class, thus if a system (or its part of degrees of freedom) belongs to the class, we can expect the relations to be satisfied even in strong couplings.

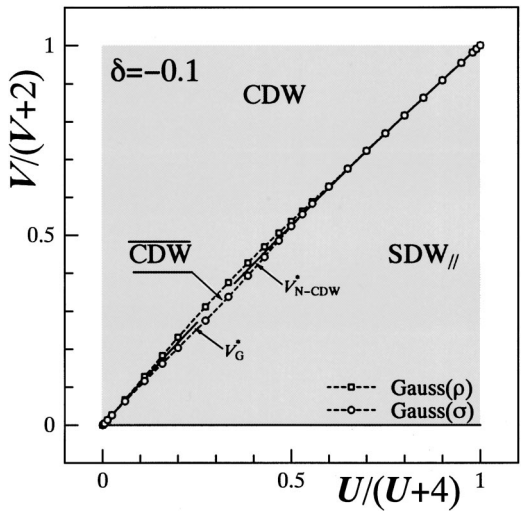

FIG. 9. Ground-state phase diagrams of the 1D AEHM at half filling: An easy-axis anisotropic case $\delta=-0.1$. Solid curves denote the analytically evaluated phase boundaries in the weak- and strong-coupling regions Eqs. (8) and (15). Squares and circles with broken lines exhibit calculated data for the Gaussian transition points in the charge and spin parts, respectively.

For the systems on the hidden-SU(2) BKT line (i.e., the spin part of AEHM with positive δ), due to the renormalization effect of the marginally irrelevant backward scattering process (g_σ), the excitation levels logarithmically split keeping the relation[21,37,38]

$$\frac{x_{\sigma,2}+3(x_{\sigma,1}\text{ or }x_{\sigma,3})}{4}=\frac{1}{2}. \tag{27}$$

On the other hand, there is a following-type duality relation among the elementary excitations on the Gaussian fixed lines

$$(x_{\nu,1}\text{ or }x_{\nu,2})\times x_{\nu,3}=\frac{1}{4}. \tag{28}$$

To calculate $x_{\nu,i}$ we should normalize $\Delta E_{\nu,i}$ by v_ν. This is done by evaluating an appropriate descendant level with the total momentum $k=2\pi/L$ in each part:

$$v_\nu=\lim_{L\to\infty}\frac{\tilde{E}_\nu-E_0}{2\pi/L}, \tag{29}$$

where $\tilde{E}_\nu$ is a lower excitation level with $S^z_{\rm T}=0$ and $N=L$. Here note that, in the SU(2)-symmetric case ($\delta=0$), $\tilde{E}_\sigma$ and primary states with the conformal spin $s_\sigma=1$ (i.e., $e^{\pm i\sqrt{2}\phi_\sigma}e^{\pm i\sqrt{2}\theta_\sigma}$) form a triplet in the $k=2\pi/L$ sector, while $\tilde{E}_\rho$ is a singlet. When the system becomes U(1) symmetric ($K_\sigma\neq 1$), the degeneracy is lifted so that the descendant level $\tilde{E}_\sigma$ provides a lower-energy excitation. Thus we shall check this δ dependence of the level structure, when calculating $\tilde{E}_\nu$.

We in our previous paper presented the data to check Eqs. (27) and (28) in weak- and intermediate-coupling regions, and observed reasonable consistencies in both charge and spin excitations (see Fig. 2 in Ref. 27). In this subsection, we thus perform the check for the spin part on the stable Gaussian fixed line in whole interaction parameter range. Results are shown in Fig. 10. Note that while we used the averaged scaling dimension $x_{\sigma,\rm av}\equiv(x_{\sigma,1}+x_{\sigma,2})/2$, same accuracy is visible for the use of $x_{\sigma,1}$ or $x_{\sigma,2}$. As a result, we find that Eq. (28) holds accurately (within 0.4% accuracy), which may serve a reliability of our calculation results also in the strong couplings. Further, the exponent $x_{\sigma,\rm av}$ converges to 1 (i.e., $K_\sigma=2$) for $U\gtrsim 10$, which shows the system to be reduced to the $S=\frac{1}{2}$ XY chain.

V. DISCUSSIONS AND SUMMARY

As we have observed in the above, the phases realized in the strong couplings, i.e., CDW, ferromagnetic, and Néel phases are classical and well characterized. However, in the weak- and intermediate-coupling regions, we have only discussed lower-energy excitations in both charge and spin parts, although the properties of electron systems are described as their composite. So we finally discuss the characters of phases by introducing relevant order parameters. The $2k_{\rm F}$ CDW and SDW are described by order parameters defined on site:

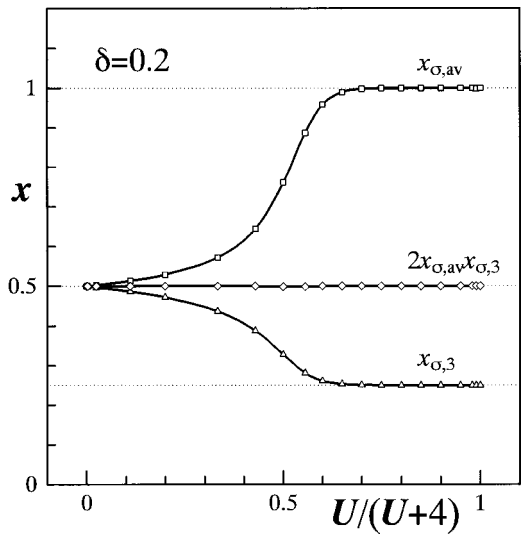

FIG. 10. Consistency check among scaling dimensions $x_{\sigma,i}$ on the stable Gaussian fixed line ($\delta=0.2$). The averaged scaling dimension is defined as $x_{\sigma,\mathrm{av}}\equiv(x_{\sigma,1}+x_{\sigma,2})/2$. Equation (28) holds within an accuracy of 0.4%.

$$\mathcal{O}_{\mathrm{CDW}}\equiv e^{i2k_{\mathrm{F}}x}n_j\propto\cos\sqrt{2}\phi_\rho\cos\sqrt{2}\phi_\sigma, \tag{30}$$

$$\mathcal{O}^{\parallel}_{\mathrm{SDW}}\equiv e^{i2k_{\mathrm{F}}x}S^z_j\propto\sin\sqrt{2}\phi_\rho\sin\sqrt{2}\phi_\sigma, \tag{31}$$

$$\mathcal{O}^{\perp}_{\mathrm{SDW}}\equiv e^{i2k_{\mathrm{F}}x}S^+_j\propto\sin\sqrt{2}\phi_\rho\exp(i\sqrt{2}\theta_\sigma), \tag{32}$$

where $\parallel$ ($\perp$) indicates a longitudinal (transverse) component of SDW and the right-hand sides show their bosonized expressions. While the order parameter correlation function decays as a power law in the $\mathrm{SDW}_\perp$ phase, there exists a long-range-order (LRO) of Eq. (30) in the CDW phase [and Eq. (31) in the $\mathrm{SDW}_\parallel$ phase]. Adding these, we shall introduce the following:[29,43,45]

$$\mathcal{O}_{\overline{\mathrm{CDW}}}\equiv e^{i2k_{\mathrm{F}}x}\overline{n}_j\propto\sin\sqrt{2}\phi_\rho\cos\sqrt{2}\phi_\sigma, \tag{33}$$

$$\mathcal{O}^{\parallel}_{\overline{\mathrm{SDW}}}\equiv e^{i2k_{\mathrm{F}}x}\overline{S}^z_j\propto\cos\sqrt{2}\phi_\rho\sin\sqrt{2}\phi_\sigma, \tag{34}$$

$$\mathcal{O}^{\perp}_{\overline{\mathrm{SDW}}}\equiv e^{i2k_{\mathrm{F}}x}\overline{S}^+_j\propto\cos\sqrt{2}\phi_\rho\,\exp(i\sqrt{2}\theta_\sigma), \tag{35}$$

where quantities with the overbar are defined ''on bonds''

$$\overline{n}_j\equiv\mathbf{c}^\dagger_j\cdot\mathbf{c}_{j+1}+\mathrm{H.c.},\quad 2\overline{S}^\mu_j\equiv\mathbf{c}^\dagger_j\cdot\sigma^\mu\cdot\mathbf{c}_{j+1}+\mathrm{H.c.} \tag{36}$$

While Eq. (30) is the CDW order parameter, Eq. (33) describes the ''bond-located'' CDW ($\overline{\mathrm{CDW}}$). Similarly, corresponding to Eqs. (31) and (32) the bond-located SDW ($\overline{\mathrm{SDW}}_{\parallel,\perp}$) can be defined by Eqs. (34) and (35). Qualitatively, the correlation functions of these order parameters behave the same as those of corresponding site-located ones. For example, LRO of Eq. (33) exists in the $\overline{\mathrm{CDW}}$ phase. When we use the terminology of the two-chain spinless fermion model in Ref. 29, a site-off-diagonal operator, e.g., the y component of $\overline{\mathrm{SDW}}$ represents a type of local current, so it corresponds to the so-called orbital antiferromagnet.

For the system with the easy-plain anisotropy, depending on the value of δ, there are four or three phases separated by two transition lines except for the ferromagnetic phase (see Fig. 8). Each can be characterized by the averages of the phase fields as

$$(\langle\sqrt{8}\phi_\rho\rangle,\langle\sqrt{8}\phi_\sigma\rangle)=\begin{cases}(\pi,*), & \mathrm{SDW}_\perp,\\ (0,0), & \mathrm{CDW}(LRO),\\ (0,*), & \overline{\mathrm{SDW}}_\perp,\\ (\pi,0), & \overline{\mathrm{CDW}}\ (\mathrm{LRO}).\end{cases} \tag{37}$$

Here ''an asterisk'' means the phase to be unlocked. Results thus show that although the previous g-ology arguments were succeeded in a prediction of upper three phases, it failed to show the existence of the long-range-ordered $\overline{\mathrm{CDW}}$ phase. Further the phase transition between the $\overline{\mathrm{CDW}}$ and ferromagnetic phases is visible in quite narrow but finite area close to the $2V=U$ line in the intermediate-coupling region. On the other hand, for a system with strong anisotropy $\delta=0.5$, since the multicritical point plunges into the ferromagnetic domain, $\overline{\mathrm{SDW}}_\perp$ directly contacts with the ferromagnetic phase, instead. We think that this observation is not due to an artificial effect in our numerical calculation procedure but is inherent in AEHM.

In the easy-axis anisotropic case Fig. 9, a strong-coupling fixed point with the averages of fields (π,π) appears where LRO of $\mathrm{SDW}_\parallel$ is established (Néel state). The direct transition between the LRO-$\mathrm{SDW}_\parallel$ and CDW phases which is a conclusion of g-ology arguments is absent in weak and intermediate couplings. Alternatively, it is observed that there exists the intermediate $\overline{\mathrm{CDW}}$ phase between them. Further, Fig. 9 exhibits that with the increase of U the area of $\overline{\mathrm{CDW}}$ phase becomes narrow and finally disappears around $U\simeq10$. Since the transition in the strong-coupling region is first order, this confluence may be naturally expected to stand for a crossover point to the first-order transition. Consequently, we think that the global structure of AEHM with the weak easy-axis anisotropy is qualitatively same as the case of EHM,[17,18] although the spin-gap transition and SDW in EHM are substituted by the Gaussian-type second-order transition and LRO-$\mathrm{SDW}_\parallel$, respectively.

To summarize, we studied global structures of the ground-state phase diagrams in the 1D anisotropic extended Hubbard model at half filling. We accurately determined the critical points by use of the numerical method, and then constructed the ground-state phase diagrams with high resolution. We closely compared our numerical calculation results for the phase boundaries with analytical estimations in three limiting regions of the Coulomb interactions, and then found a good agreement between them. On the other side, in the intermediate-coupling region, we observed a richness of

structures in the phase diagrams: In the easy-plain anisotropic case, the regions where bond-located spin- and charge-density waves become dominant were determined, and the phase transition between the complete ferromagnet and one of these phases was observed (the phase contacting with the ferromagnetic region depends upon the anisotropy parameter value). In the easy-axis anisotropic case, we found that the structure of the phase diagram is same as that of the isotropic extended Hubbard model. To serve a reliability of our calculations, we also checked consistencies among excitations.

ACKNOWLEDGMENTS

The author is indebted to M. Nakamura for providing his preprint prior to publication as well as for discussions of numerical calculations using the level-spectroscopy method. He is also grateful to Y. Okabe for helpful discussions. Main computations were performed using the facilities of Tokyo Metropolitan University, Yukawa Institute for Theoretical Physics, and the Supercomputer Center, Institute for Solid State Physics, University of Tokyo.

*Email address: otsuka@phys.metro-u.ac.jp

[1] J. Kanamori, Prog. Theor. Phys. **30**, 275 (1963); J. Hubbard, Proc. R. Soc. London, Ser. A **276**, 238 (1963); M.C. Gutzwiller, Phys. Rev. Lett. **10**, 59 (1963).
[2] S. Tomonaga, Prog. Theor. Phys. **5**, 544 (1950); J.M. Luttinger, J. Math. Phys. **4**, 1154 (1963).
[3] F.D.M. Haldane, J. Phys. C **14**, 2585 (1981).
[4] H. Frahm and V.E. Korepin, Phys. Rev. B **42**, 10 553 (1990); N. Kawakami and S.-K. Yang, Phys. Lett. A **148**, 359 (1990).
[5] P.W. Anderson, Phys. Rev. Lett. **64**, 1839 (1990).
[6] R. Neudert *et al.*, Phys. Rev. Lett. **81**, 657 (1998).
[7] B. Fourcade and G. Spronken, Phys. Rev. B **29**, 5089 (1984); **29**, 5096 (1984).
[8] V.J. Emery, in *Highly Conducting One-Dimensional Solids*, edited by J. T. Devreese *et al.* (Plenum, New York, 1979), p. 327.
[9] R.A. Bari, Phys. Rev. B **3**, 2622 (1971).
[10] J.E. Hirsch, Phys. Rev. Lett. **53**, 2327 (1984); Phys. Rev. B **31**, 6022 (1985).
[11] H.Q. Lin and J.E. Hirsch, Phys. Rev. B **33**, 8155 (1986).
[12] J.W. Cannon and E. Fradkin, Phys. Rev. B **41**, 9435 (1990); J.W. Cannon, R.T. Scalattar, and E. Fradkin, *ibid.* **44**, 5995 (1991).
[13] V. Wass, H. Büttner, and J. Voit, Phys. Rev. B **41**, 9366 (1990).
[14] N. Tomita, A. Ikawa, and H. Fukutome, J. Phys. Soc. Jpn. **65**, 195 (1996).
[15] J. Voit, Phys. Rev. B **45**, 4027 (1992).
[16] P.G.J. van Dongen, Phys. Rev. B **49**, 7904 (1994).
[17] M. Nakamura, J. Phys. Soc. Jpn. **68**, 3123 (1999).
[18] M. Nakamura, Phys. Rev. B **61**, 16 377 (2000).
[19] K. Nomura, J. Phys. A **28**, 5451 (1995).
[20] R. Jullien and F.D.M. Haldane, Bull. Am. Phys. Soc. **28**, 344 (1983).
[21] K. Okamoto and K. Nomura, Phys. Lett. A **169**, 433 (1992); K. Nomura and K. Okamoto, J. Phys. A **27**, 5773 (1994).
[22] M. Nakamura, K. Nomura, and A. Kitazawa, Phys. Rev. Lett. **79**, 3214 (1997); M. Nakamura, J. Phys. Soc. Jpn. **67**, 717 (1998); M. Nakamura, A. Kitazawa, and K. Nomura, Phys. Rev. B **60**, 7850 (1999).
[23] H. Otsuka, Phys. Rev. B **57**, 14 658 (1998).
[24] A. Kitazawa, K. Nomura, and K. Okamoto, Phys. Rev. Lett. **76**, 4038 (1996).
[25] W. Chen and K. Hida, J. Phys. Soc. Jpn. **68**, 2779 (1999).
[26] T. Tonegawa, K. Okamoto, T. Hikihara, Y. Takahashi, and M. Kaburagi, cond-mat/9912482 (unpublished).
[27] H. Otsuka, Phys. Rev. Lett. **84**, 5572 (2000).
[28] For a review, see B.I. Halperin and T.M. Rice, in *Solid State Physics*, edited by F. Seitz *et al.* (Academic, New York, 1968), Vol. 21, p. 116.
[29] A.A. Nersesyan, Phys. Lett. A **153**, 49 (1991).
[30] A. Luther and I. Peschel, Phys. Rev. B **9**, 2911 (1974).
[31] For a recent review, see A.O. Gogolin, A.A. Nersesyan and A.M. Tsvelik, *Bosonization and Strongly Correlated Systems* (Cambridge University Press, Cambridge, England, 1998).
[32] V.L. Berezinskii, Zh. Éksp. Teor. Fiz. **61**, 1144 (1971) [Sov. Phys. JETP **34**, 610 (1972)]; J.M. Kosterlitz and D. J. Thouless, J. Phys. C **6**, 1181 (1973); J.M. Kosterlitz, *ibid.* **7**, 1046 (1974).
[33] J. des Cloizeaux and M. Gaudin, J. Math. Phys. **7**, 1384 (1966); C.N. Yang and C.P. Yang, Phys. Rev. **150**, 321 (1966); **150**, 327 (1966).
[34] J.D. Johnson, S. Krinsky, and B. McCoy, Phys. Rev. A **8**, 2526 (1973).
[35] A. Luther and I. Peschel, Phys. Rev. B **12**, 3908 (1975).
[36] J.L. Cardy, J. Phys. A **17**, L385 (1984); J.L. Cardy, Nucl. Phys. B **270**, 186 (1984).
[37] I. Affleck, D. Gepner, H.J. Schulz, and T. Ziman, J. Phys. A **22**, 511 (1989).
[38] T. Giamarchi and H.J. Schulz, Phys. Rev. B **39**, 4620 (1989).
[39] M. Ogata, M.U. Luchini, S. Sorella, and F.F. Asaad, Phys. Rev. Lett. **66**, 2388 (1991).
[40] The situation is same as the phase-separation transition of an extended Hubbard model discussed in Ref. 18, where the charge degrees of freedom are concerned.
[41] S. Hirata and K. Nomura, Phys. Rev. B **61**, 9453 (2000).
[42] M. Nakamura, K. Itoh, and N. Muramoto, cond-mat/0003419 (unpublished).
[43] For example, G.I. Japaridze and A.P. Kampf, Phys. Rev. B **59**, 12 822 (1999), and references therein.
[44] D.K. Campbell, J.T. Gammel, and E.Y. Loh, Jr., Phys. Rev. B **42**, 475 (1990).
[45] G.I. Japaridze, Phys. Lett. A **201**, 239 (1995).